Theoretical insights into inorganic-organic intercalation products of the layered perovskite $HLaNb_2O_7$: perspectives for hybrid proton conductors

Stefania Di Tommaso[1,2], Francesco Giannici[1,*], Adriana Mossuto Marculescu[1], Alessandro Chiara[1], Cristina Tealdi[3], Antonino Martorana[1], Frédéric Labat[2], Carlo Adamo[2,*]

1 - Dipartimento di Fisica e Chimica, Università degli Studi di Palermo, Viale delle Scienze ed. 17, I-90128 Palermo, Italy

2 - Institut de Recherche de Chimie de Paris CNRS Chimie ParisTech, 11, rue Pierre et Marie Curie, F-75005 Paris, France

3 - Dipartimento di Chimica, Università di Pavia, via Taramelli 12, Pavia, Italy

Abstract

The modification of metal oxide surfaces with organic moieties has been widely studied as a method of preparing organic-inorganic hybrid materials for various applications. Among inorganic oxides, ion-exchangeable layered perovskites are particularly interesting, in reason of appealing electronic and reactive properties. In particular, their protonated interlayer surface can be easily functionalized with organic groups allowing the production of stable hybrid materials. As a further step in the design of new inorganic-organic hybrid proton conductors, a combined experimental and theoretical study of two intercalated compounds (propanol and imidazole) in $HLaNb_2O_7$ is presented here. A generally very good agreement with the available experimental data is found in reproducing both structural features and ^{13}C-NMR chemical shifts, and marked differences between the two considered intercalated compounds are evidenced, with possible important outcomes for proton conduction. Notably, the imizadole molecules are easily protonated by the acidic protons present in the interlayer spacing, thus inhibiting an efficient charge transport mechanism.

*corresponding authors: francesco.giannici@unipa.it; carlo.adamo@chimie-paristech.fr

1. Introduction

In the last decades, the research efforts on proton-conducting electrolytes for use in hydrogen technology have been focused on two main fields: low-temperature polymer membranes (e.g. Nafion) and high-temperature oxides (e.g. barium zirconate).[1] The intermediate temperature range, also known as the "temperature gap", is not thoroughly covered by a particular class of materials, and has attracted a certain interest in recent years[1]. In particular, to overcome chemical resistance and thermal degradation issues, and to improve the overall conductivity, a growing interest has recently appeared in finding alternative approaches towards new proton conductors.[2-9] By joining organic and inorganic parts, either mixed or chemically bonded together, one may achieve the advantages of both kinds of materials in terms of thermal resistance, chemical flexibility, and high conductivity. Proton-conducting composite materials have been prepared in a wide variety of chemical and morphological combinations. Alongside the classical examples of Nafion composite membranes with inorganic fillers[2-4], many and diverse examples appeared in the recent literature, ranging from sulfonated porous silica, to MOF-polymer nanofibers[5-9].

Among other materials, perovskites were recently used as building blocks for the development of hybrid (organic/inorganic) systems. Indeed, the intercalation of molecules or ions, or the relatively easy functionalization of such materials open new perspectives[10].

In this line and with the aim to pinpoint the structural and electronic features of novel organic/inorganic hybrid materials, we studied in this work some intercalation products of the Dion-Jacobson perovskite $HLaNb_2O_7$ (HLN), a solid acid showing a layered structure in which 2-dimensional nanosheets with the $LaNbO_3$ perovskite structure are stacked and separated by H^+ layers[11,12]. The internal surfaces of this layered oxide show, indeed, good reactivity with a large variety of organic compounds, forming (Nb-)O-C covalent bonds. In particular, the distance between the perovskite sheets was expanded by reaction with various *n*-alcohols[13,14], and other organic moieties, such as organophosphonic acids[15], trifluoroacetate groups[16] and glucose[17]. Alkylamines and pyridine were also reported to be intercalated in HLN, due to the acidity of the interlayer H^+ ion[18,19]. In particular, we have recently reported the fast intercalation of imidazole, histamine, and 3-mercaptopropyl-trimethoxysilane inside HLN using sonochemical methods[20].

Due to a wide variety of compositions, a basic understanding of the relations between structure and function is a prerequisite for any technological application of such hybrid materials. Therefore, as a first step toward more complex systems, we have performed a combined experimental and theoretical investigation of two hybrid HLN materials, obtained

by the intercalation of two simple molecules, namely 1-propanol and imidazole. These hybrid materials will be referred to as **Pro-HLN** and **Imi-HLN** in the following.

The first material, already experimentally prepared in literature[14], represents a simple benchmark for testing our protocol, whereas the second is a prototype for a proton-conducting hybrid. Indeed, imidazole molecules represent a simple yet effective proton conductor and they have been confined in several organic and inorganic systems in order to obtain better-performing membranes[21-23].

The aim is to fully characterize these relatively simple systems, both at experimental and theoretical levels. Indeed, HLN represents an ideal scaffold for functionalization, since its ordered arrangement of nanosheets can be modeled systematically at the theoretical level. Nevertheless, while several experimental studies exist on the synthesis and characterization of intercalation HLN products, a detailed theoretical analysis of the same compounds is still missing. The interplay between experimental and theoretical methods then provides a thorough understanding for further development of this class of functionalized materials.

To this end, we consider: a) the atomic structure in terms of interlayer distance (XRD), density of the organic moieties between the nanosheets (TGA), and their arrangement; b) the electronic structure, especially on the nature of the chemical bonds (covalent, ionic, hydrogen bonding) between the perovskite and organic moieties; c) ^{13}C-NMR chemical shifts of intercalated molecules. The understanding of structural and electronic properties of these hybrid materials will provide useful information to introduce proton-carrying groups between the HLN nanosheets, and eventually to design novel hybrid proton conductors.

2. Materials and methods

2.1 Synthesis and experimental characterization

$HLaNb_2O_7$ (HLN) was prepared by treating $RbLaNb_2O_7$ with aqueous HNO_3 (6M) at 60 °C for 72 h. The powder was centrifuged, washed with distilled water, filtered under vacuum on a membrane filter, and dried at 80°C overnight[14]. **Pro-HLN** and **Imi-HLN** were synthesized by using a sonochemical method developed by our group[20].

Pro-HLN was prepared by adding HLN to a mixture of water and n-propanol (3:25 volume ratio), and treating in an ultrasonic bath for 8 hours at room temperature. Afterwards, the mixture was stirred at 80°C for 3 d under reflux. The product was recovered by filtration and dried under vacuum. **Imi-HLN** was prepared by dispersing HLN and imidazole in a mixture of water and tetrahydrofuran (1:40 volume ratio), and treating in an ultrasonic bath for 10 hours at room temperature. The product was recovered by filtration and dried under vacuum.

For full details on the materials preparation, see reference 20. X-Ray Diffraction (XRD) patterns were acquired with a Siemens D500 diffractometer in Bragg-Brentano geometry, using Cu-Kα radiation, and a graphite monochromator on the diffracted beam. Solid-state ^{13}C-NMR spectra were recorded on a Bruker Avance III spectrometer using cross-polarization and magic angle spinning techniques (CP/MAS) at 100.61 MHz. Thermogravimetric analysis (TGA) was carried out up to 700°C under dry nitrogen flux with a TA Q5000 analyzer.

2.2 Computational details

The structure optimizations have been carried out using the CRYSTAL09 code[24] in its massively parallel (MPP) version[25], allowing to efficiently compute the electronic structure of periodic (and non periodic) systems by means of methods rooted in Density Functional Theory. Starting from our previous work on the Dion-Jacobson layered perovskites, MLaNb$_2$O$_7$ (with M monovalent cations)[26], different exchange-correlation functionals have been tested in this work. They include Generalized Gradient Approximations, such as the Perdew-Burke-Ernzerhof (PBE)[27] and the SOGGA functionals[28], and hybrids approaches, such as B3LYP and PBE0[29-31], containing respectively 20 and 25% of HF exchange. These latter's were also empirically corrected for dispersion, using the D2 correction due to Grimme (B3LYP-D and PBE0-D in the following)[33]. On the basis of the performance analysis the B3LYP functional was selected and its results discussed in the paper (see SI for details and further discussion).

Hay and Wadt small core pseudopotentials have been chosen for Nb^{+5} and La^{+3}, along with 31(31d)G and a 411(1d)G basis set, respectively, for valence electrons[34]. O^{2-} anion has been described using a large core Durand and Barthelat pseudopotential[35] with a double-ζ split valence basis set. Concerning the organic moieties, triple-ζ split valence basis sets with polarization have been chosen for hydrogen[36], carbon and nitrogen[37].

All NMR calculations were carried out using the Gaussian 09 program[38], by cutting clusters from the optimized periodic structures. Following a consolidate procedure, they were carried out within the GIAO formalism[39], using the hybrid functional B3LYP. IGLO-III basis set[40] have been considered for C, O, H and N atoms, while Los Alamos effective core pseudopotential and a double-ζ basis set were selected for La and Nb[41]. Chemical shifts were computed with respect to tetramethylsilane shieldings obtained at the same level of theory.

3. Results and discussion

3.1 Synthesis and characterization

The enlargement of the interlayer spacing is followed with XRD, which gives a first indication of the successful intercalation of organic molecules between the HLN layers. As shown in Figure 1, by comparison of the intercalated compounds with the parent HLN oxide, the (001) Bragg peak is shifted to lower angles, thus confirming the intercalation. The periodicity along the z-axis derived from XRD peak indexing is 15.38 Å for **Pro-HLN**, and 13.99 Å for **Imi-HLN**.

To obtain quantitative information about the organic molecules content, TGA experiments were performed on the functionalized samples. HLN layers undergo a structural rearrangement at 500°C, according to the following reaction:

$2\ HLaNb_2O_7 \rightarrow La_2O_3 + 2\ Nb_2O_5 + H_2O$

which accounts for a weight loss of 2.06%. In this way, the weight loss due to the thermal decomposition of organic moieties is determined as the difference with respect to the total weight loss. In our cases, this procedure leads to a weight loss of 3.97% and 5.66% in **Pro-HLN** and **Imi-HLN**, respectively. These values give also an indication of the average surface coverage. In **Pro-HLN**, 0.4 propanol molecules are intercalated per HLN unit formula, while in **Imi-HLN**, 0.4 imidazole molecules are intercalated per HLN unit formula. One should keep in mind that these values represent an average over the different zones in the sample and, of course, there might also be zones with a different coverage.

Solid state ^{13}C-NMR confirms that n-propanol binds with the interlayer surface by forming a (Nb-)O-C covalent bond, as indicated by the large change of the carbon C1 (see figure 2 also for atoms labels) chemical shift from about 63 ppm in free n-propanol to about 80 ppm in **Pro-HLN**. These results are in good agreement with the previous results of Suzuki et al.[14] obtained for the same compound, and indicate that no free n-propanol molecules are present in the interlayer.

Imidazole, on the other hand, does not seem to form covalent bonds with the surface, as the ^{13}C-NMR spectrum does not indicate very large differences between pure and intercalated imidazole. As what concerns the protonation of the azole ring, the ^{13}C-NMR spectrum of **Imi-HLN** shows one peak at 135 ppm, and a splitted peak around 120-123 ppm. In literature, it has been shown that the ^{13}C-NMR spectrum of pure solid imidazole presents three distinct peaks, at 137, 128 and 116 ppm, attributed to C2, C4 and C5, respectively. Protonated imidazole (imidazolium cation), only shows two peaks instead, at 135 and 121 ppm, since C4 and C5 are equivalent in this case[42]. The comparison between our results and the data already shown in literature indicates that in **Imi-HLN**, imidazole is intercalated as imidazolium cation, ionically bound with the HLN interlayer surface[20].

2. *Theoretical characterization*

From a theoretical viewpoint two different settings have been tested for the structural and electronic characterization of the hybrid compounds, as sketched in figure 3. In the first arrangement, the *surface* model (labeled **HLN**$_s$), the organic molecule is adsorbed on the oxide exposing the interlayer surface. For the first model, regardless of the organic molecule, structures have been directly derived from HLN keeping the tetragonal (*P4*) symmetry of the precursor material. **HLN**$_s$ are, indeed, two-dimensional periodic systems obtained by cutting the bulk structure of HLN along the (001) surface exposing the interlayer protons: the nonperiodic direction is the one perpendicular to the surface plane (along the *c* axis).

As already discussed in the previous section on the basis of the XRD results, the intercalation of organic molecules happens between two perovskite slabs. Therefore a second model (**HLN**$_b$) was considered, to take into account the confinement effect on the interlayer adsorption of the molecule. This model was obtained by enlarging the interlayer spacing of the precursor material and adding the organic moiety between the perovskite layers. In this case, the structure is periodic in three directions, with symmetry lowered from tetragonal to triclinic (*P1*). Note that in this case, the structure was obtained by enlarging the size of the HLN cell (from 1x1x1 to 2x2x1 or to 2x3x1) in order to reproduce the experimentally determined coverage.

Pro-HLN

The first model system, labeled **Pro-HLN**$_b$ in figure 4, was built by introducing one propanol molecule into the interlayer space of a 2x2x1 cell. This structure corresponds to 0.25 propanol molecules intercalated per HLN unit formula, not too far from the experimental value (θ=0.4, see above), giving a unit cell about two times larger than HLN[26] in the c direction. As can be seen from the data collected in table 1, the substitution of one proton with propanol induces a significant increase of the interlayer distance (c parameter), which goes from 10.43 Å (from reference 26) to 13.51 Å. The other two lattice parameters, *a* and *b*, are almost two times those of the parent HLN (see table 1), thus suggesting that they are not affected by the cell doubling. Furthermore, a pseudo-tetragonal structure is retained, the α, β and γ angles being fairly close to the expected 90° value. Table 2 collects the interatomic cell parameters for **Pro-HLN**$_b$ and the reference HLN protonated species. The average value of the Nb-O distances increases for all the three bonds (equatorial, axial long and short), but the largest deviations concern the bonds along the c direction. Indeed, a +0.07 Å lengthening is observed for the

mean bond lengths, while the largest increase is +0.22 Å for the Nb-O axial bond (see table 2 for details). Concerning the organic moiety, the Nb-O-C angle is around 180° and there is a very small overlap between the alkyl chain and the upper (non-bound) perovskite layer. As mentioned above, the organic molecule does not induce any significant distortion of the two inorganic slabs, apart from the protons on the surfaces, all pointing toward the vicinal non-protonated oxygen atoms (see figure 4).

From an experimental point of view, apart from the ^{13}C-NMR spectrum that ensures that the molecule is covalently bound to the surface, the XRD analysis allows to estimate that the *c* parameter is equal to 15.4 Å, in agreement with previous experimental data[14]. The large underestimation obtained with the B3LYP functional (13.5 vs. 15.4 Å) induced us to consider other DFT approaches, even if we have already shown that the structure of the protonated perovskite (HLN) is correctly reproduced at this level of theory[26]. The results obtained with different functionals are collected in table S1. The error in the description of the *c* lattice parameter is significant with all the functionals considered. Indeed, an underestimation is always found, which ranges from -2.5 Å (PBE0) to -3.1 Å (SOGGA) with respect to the XRD data. Moreover, unlike our findings for the non-functionalized HLN[26], the addition of the Grimme's empirical correction for dispersion (D) increases dramatically the underestimation of the interlayer spacing, reaching an error discrepancy of about 4 Å (PBE0-D). In this latter case, the structure obtained presents an Nb-O-C1 angle of 156.2° with the molecule laying on the interlayer surface. In addition, the organic moiety is well inserted in the cavity formed by the four NbO_6 of the upper perovskite layer, resulting in highly distorted octahedra with a significant underestimation of the interlayer spacing (see figure S2).

The nature of the chemical bond between the surface and the propyl group is confirmed by the density of states (DOS) of the system, computed at the B3LYP level and reported in Figure 5. The calculated direct electronic band gap of 3.29 eV is comparable to the one calculated for the non functionalized HLN (about 3 eV)[26]. Looking at the partial DOS relative to the atoms belonging to the inorganic part of the compound (O_{2p}, Nb_{4d} and La), they are in qualitative agreement (i.e. position of the different contributions to the total DOS) with previous computational results on HLN[26,43]. The O_{2p} and Nb_{4d} contribute largely to the DOS, thus underlining the Nb-O covalent bonds building up the octahedra of the inorganic slabs. Furthermore, the partial DOS of lanthanum reaches its maximum values around -15 (not shown) and 10 eV, and its contribution, in both peaks, almost overlaps the dotted line representing the total DOS: this clearly indicates a purely atomic contribution of La to the DOS. In what concerns the partial DOS of the propyl group, the contribution of the organic

part of the system is present in a wide energy range, going from 0 to about -6 eV, in the valence band and overlaps the oxygen contribution in all the indicated range. This confirms the covalent nature of the interaction between the inorganic and organic parts of the hybrid system. Mulliken charges (table S5) further confirm this finding, the propanol bearing a charge of +0.37 e.

Starting from these results, a bulk structure of the HLN functionalized with two different propyl groups (**2Pro-HLN*b***, Figure 4) was built. In this case, different conformations of the two organic moieties lead to different structures collected in table S1, characterized by different cell parameters and relative stabilities. In the most stable rearrangement, the two propanol molecules are bound to two non-equivalent oxygen atoms, and lay on the inner perovskite surfaces, the O-C-C-C dihedral angle being about 59°. More interestingly the interlayer distance increases by 0.6 Å and the two inorganic layers slide in opposite directions along the *b* axis, thus losing any symmetry, as indicated by the β angle (now 72.8°). The deformation of the cell induced by the two propanol molecules does not affect the interatomic distances, which do not significantly change with respect to the **Pro-HLN*b*** case (see table 2).

The other structures, significantly higher in energy, are characterized by even larger interlayer distances (up to 18.9 Å), due to the repulsion between the organic moieties, more extended and/or close to each other (see table S1). As before, a check of the results was carried out using different functionals. In particular, B3LYP-D calculations were carried out on all the structures identified at B3LYP level and the results are collected in table S3. All these structures present interlayer distances shorter than the experimental value and the B3LYP analogues.

In the double intercalation model **2Pro-HLN*b***, the propanol/HLN ratio is higher than the experimental data, being 0.5 instead of 0.4 found from the TGA analysis of the synthesized compound. A new structure was then obtained by enlarging the size of the HLN supercell (from 2x2x1 to 2x3x1), leading to a coverage of 0.34. The most stable structure was optimized using several DFT approaches (see table S3). Regardless of the functional considered, adding a second propyl group increases the interlayer spacing toward the experimental value derived from the XRD analysis (15.4 Å). Consistently with the previous discussion, the best *c* length has been still obtained using B3LYP (14.4 Å) while the worst with the PBE0-D functional (12.0 Å). Consequently, as already found and discussed for **Pro-HLN*b***, the *c* parameter is underestimated with all the functionals considered here.

Even if these data consolidate the choice of B3LYP as the most reliable functional for our systems, still a discrepancy between the theoretical and experimental interlayer distance is

present (14.4 vs. 15.4 Å). As can be seen from the data reported in table S1, a second structure, characterized by a longer interlayer distance (16.2 Å) lies at 3.2 kcal/mol higher in energy. It can then be argued, taking into account the methodological error on both distances and relative energies, that also this structure is accessible. Therefore, the experimental result, midway between 14.4 and 16.2 Å, could also arise from the average of two or more different configurations. These results also show that empirical corrections significantly overestimated dispersion interactions leading to short non-bonding, in agreement with previous results on solid state systems[44,45].

In order to have a complete picture of the alcohol-perovskite interaction, a surface model has also been considered. In this **Pro-HLN**$_s$ model (see Figure 4), only the perovskite layer on which the organic part is directly bound has been considered, and only three first atomic layers of the inorganic part (i.e. surface protons, oxygen and niobium atoms) and the organic part were relaxed during geometry optimization. In fact, it was verified that optimizing additional layers does not change remarkably the final optimized structure. Apart from a general reorientation of the surface OH group and of the oxygen atoms on the (001) exposed surface, due to the interaction (attractive and/or repulsive) with the alkyl chain, the perovskite slab is not highly affected by the presence of the organic group covalently bound on the external surface. The major effects of the optimization are on the structure of the organic part of the hybrid system. In fact, due to the absence of the upper perovskite layer, a drastic bending of the organic moiety toward the surface can be observed, the Nb-O-C1 angle being 152.9° instead of 175.9°, as obtained with B3LYP for **Pro-HLN**$_b$. This 2D model of the intercalated compound, lacking the upper perovskite slab, obviously prevents from evaluating the *c* cell parameter.

Starting from these structures, several clusters were extracted in order to compute ^{13}C-NMR parameters (see Figure 6). In particular, three clusters were built: cluster 1 is formed by the propyl group sandwiched between two layers of four NbO_6 octahedra, and was obtained by cutting the bulk model optimized structure (**Pro-HLN**$_b$); cluster 2 is composed by the propyl group and just one layer made of four NbO_6 octahedra. Finally, cluster 3 was directly derived from the surface model structure (**Pro-HLN**$_s$).

From table 3, a good agreement between experimental and theoretical values emerges, with deviations always lower than the expected mean error for this level of theory (about 15 ppm, see reference 46), for all the considered systems models. Looking more in detail, in cluster 1, the C1 and C2 chemical shifts are overestimated by about 9 ppm, while a better agreement between theory and experiment is found for C3 (16.8 vs 12.5 ppm). A marginal improvement

is obtained in cluster 2, while with cluster 3 a definitely substantial agreement is eventually found, with differences of about 3.0 ppm for C1 and C2 and of only 1.1 ppm for C3. These latter results confirm the effect of the underestimation of the interlayer distance when computing NMR properties. A further re-optimization of this cluster has a marginal effect on the C1 and C3 chemical shifts. Other functionals (SOGGA, PBE, PBE0 and PBE0-D) do not provide better agreement with experimental data (see table S4).

These results on the propanol/perovskite hybrid system indicate, beyond the good agreement between theoretical and experimental data, that the organic molecule is covalently bond to the interlayer surface, but the electronic properties of the original inorganic moiety are preserved.

Imi-HLN

Starting from the results obtained for **Pro-HLN** and as already described for this latter hybrid system, the intercalated compound with imidazole has been considered in two different ways: inclusion in the interlayer spacing and two-dimensional adsorption on the surface. Both models were optimized using the B3LYP functional and the optimized structures are reported in Figure 4, while the corresponding cell parameters are in table 3.

Imi-HLN*b* was obtained by intercalating one imidazole molecule in the interlayer spacing of a 2x2x1 HLN supercell, corresponding to a coverage of 0.25 imidazole molecules per HLN unit formula. As far as the inorganic part is concerned, the optimized B3LYP structure of the compound is highly distorted due to the presence of the imidazole. In particular, due to the interaction of the NH group of imidazole with a non protonated oxygen atom facing the interlayer spacing, the upper slab is displaced along the *ab* plane, with an α angle of 103.6° (for **Pro-HLN*b*** the value for the same angle is 95.8°). Both in the lower and in the upper slab the octahedra appear strongly tilted and the niobium-axial oxygen distances are alternately elongated (around 2.5 Å, with the oxygen atoms facing the lanthanum layer) and shortened (1.8 Å, toward the interlayer spacing) with respect to the average of about 2 Å measured for the Nb-O equatorial bonds (see table 2). This latter is a feature of the inorganic support, already underlined in our previous work on the precursor material[26].

Concerning the organic part of the system, the intercalated imidazole after the optimization is protonated by one of the acidic protons of the HLN interlayer region. The resulting imidazolium ion is inclined in the interlayer spacing (O-N1-N2=156.56°, considering N1 the nitrogen atom nearest to the lower interlayer surface, table 4), being affected by the deprotonated oxygen atom present on both the inner surfaces of the perovskite slabs (the (N)H-O distances are 1.62 and 1.66 Å with the lower and the upper surface, respectively).

These interactions implicate that the *c* parameter of the unit cell of **Imi-HLN*b*** is well described in spite of the different (lower) coverage considered in this first model. In fact, as already discussed, from an experimental point of view, the XRD analysis allows the estimation of 13.99 Å for the **Imi-HLN** *c* parameter, obtained for an imidazole/HLN ratio of 0.34, while in this first model we obtain 13.98 Å for a coverage of 0.25.

Also in this case, the plot of the partial and total DOS of the compound (Figure 5) confirms and elucidates the nature of the interaction between the organic and the inorganic part of the hybrid compound. The electronic gap calculated between valence and conduction band of the whole system is equal to 3.07 eV comparable with the one computed for the previous compound as well as for HLN (about 3.0 eV)[26]. The position and the trend of the partial DOS relative to the atoms of the inorganic slab are very similar to the one already discussed for **Pro-HLN**.

A significant difference between the two hybrid systems is highlighted by the contribution of the organic part to the DOS. Differently from the case of propanol, the overlap of the organic and inorganic contributions to the total DOS shows two weakly interacting parts in the whole system, especially in the valence band (see Figure 5). In particular, focusing on the partial DOS of imidazole, it only slightly overlaps the oxygen (2p) contribution in the valence band, suggesting a much weaker bonding between the molecule and the surface than in the **Pro-HLN** case. Moreover, a purely organic contribution to the total DOS can be seen near the Fermi level: this represents the Highest Occupied Crystalline Orbital (HOCO) of the hybrid system that is completely localized on imidazole (see figure S3). Mulliken atomic charges (table S5) indicate that the imidazole has a strong positive charge (+0.8 e), due to its protonated state.

When considering the second model, **2Imi-HLN*b***, consisting of a 3x2x1 HLN supercell intercalated with two imidazoles (1 imidazole/3 HLN unit formula), the experimental value of coverage (0.34 imidazole/HLN) is reached. In this compound, the structure is less distorted than in the case of the mono-intercalated one. In particular, the two perovskite slabs do not shift in the *ab* plane (the α angle is in this case 89.75°) and the NbO_6 octahedra are not tilted. As far as the organic part is concerned, both imidazoles are protonated by the HLN surface protons and the shortest distance between the two heterocycles is around 2.4 Å. Moreover, analogously to what already shown for **Imi-HLN*b***, the position of the derived imidazolium in the interlayer space is driven by the interaction between the two N-H groups of each ion and the deprotonated oxygen present on the inner surfaces, with distances of around 1.6 and 1.7 Å with the lower and upper slab respectively. Furthermore, the inclination of the molecules with

respect to the surfaces are comparable with the ones discussed above for the previous hybrid compound (Table 4). It is the presence of the two molecules and, above all, the doubling of the attractive interactions in the interlayer spacing, that cause the underestimation of about 0.5 Å of the *c* parameter, in spite of the correct value of coverage.

For the *surface* model, a 3x3 supercell was obtained from HLN and a neutral imidazole free to diffuse was inserted at the center of the supercell parallel to the surface at about 2 Å distance from the protons. In the optimized structure of **Imi-HLN**$_s$ reported in Figure 4, the imidazole is displaced from the center of the super cell, due to the interaction between the molecule and the surface, dominated, in this case, by strong hydrogen bonds.

The structure of the inorganic part of the hybrid compound, apart from the reorientation of the surface OH groups due to the presence of the molecule, is unchanged after optimization. Contrary to the evidences obtained for the bulk model, in **Imi-HLN**$_s$ imidazole is not protonated by the acidic surface protons, and the distance between the non protonated nitrogen atom and the nearest proton of the surface is 1.85 Å. Furthermore, the molecule is less inclined than in the previous model (O-N1-N2 is equal to 117.52°, Table 4) due to the attractive interactions between the proton of the imidazole and the oxygen atoms of the surface.

As what concerns the NMR chemical shifts, the results of different clusters are reported in Table 3 along with the experimental data. As already discussed for **Pro-HLN**, cluster 1 is made up of the imidazole sandwiched between two layers of four NbO_6 octahedra, and was cut from the optimized structure **Imi-HLN**$_b$; cluster 2 is composed by the imidazole and just one layer made up of four NbO_6 octahedra, and was obtained from the surface model optimized structure **Imi-HLN**$_s$. Cluster 3 was obtained from the optimized bulk structure by removing the upper perovskite slab (the cluster structures are shown in the Supporting information).

From table 3, it is clear that cluster 1 is the one giving the best description of the intercalated imidazole ^{13}C-NMR shieldings. Starting from the results discussed previously, this is not surprising. In fact, it was shown that the optimized bulk model structure of **Imi-HLN**$_b$ allows to reproduce the correct distance between the two perovskite slabs (not considered in cluster 3) and the protonation of imidazole.

For C2, the carbon between the two nitrogen atoms, a chemical shift of about 138 ppm was found by calculation, with a difference of about 3 ppm with respect to the maximum of the experimental peak (around 135 ppm).

The atoms C4 and C5, in the hybrid compound, are symmetric as in the case of an imidazolium ion (in that case, we computed for the two atoms the same chemical shift of 131 ppm at the same level of theory). The difference between these two shifts (of about 2 units) is due to the interaction of the CH groups with the surfaces. In particular, the hydrogen bound to C4 interacts with two different oxygen atoms of the upper perovskite slab (with distances H-O from 2.4 to 2.9 Å). On the other hand, the hydrogen bound to C5 interacts with one unprotonated oxygen of the interlayer surface with a distance of 2.4 Å. This difference between the two carbon atom shifts, and the corresponding loss of symmetry are compatible with the broad signal registered in the experimental spectrum of **Imi-HLN** (Figure 2) between 116 and 124 ppm, that was previously discussed.

These results give some valuable insights on the possible development of hybrid imizadole/perovskite materials as proton conducting membranes. The mechanism commonly accepted to explain directional proton molecular transport requires a well-structured H-bond network among non-protonated imidazoles. This network allows a Grotthuss diffusion mechanism, where the charge carrier (here an excess proton) jumps from an imidazole to the adjacent one[47,48]. Such mechanism is very effective in free or almost-free imidazoles[49]: on the contrary, both experimental and theoretical data suggest that the imidazoles present in **Imi-HLN** are easily protonated, thus hampering an efficient transport mechanism. A possible way out could be to add a linker between the surface and the charge carrier[50] in order to reduce protonation effects from the surface. In this case, however, the stability of the resulting hybrid material could be a major issue.

4. Conclusions

In this work, we presented a combined experimental and theoretical study aiming at a comprehensive characterization of two hybrid compounds obtained from the intercalation of organic molecules, propanol and imidazole, in the layered perovskite $HLaNb_2O_7$ (HLN).

In particular, while the syntheses of **Pro-HLN** and **Imi-HLN** were already reported on by us, this work represents the first combined theoretical/experimental characterization on the intercalation of organic molecules in the HLN interlayer spacing. The structural characterization was carried out by means of XRD, which highlights intercalation by giving evidences of the enlargement of the interlayer distance; TGA, allowing the quantitative evaluation of the degree of functionalization of the inorganic support, and solid state ^{13}C-NMR, to obtain insights about the conformation of the organic part of hybrid systems.

From a theoretical point of view, the characterization of the electronic structure of the hybrid compounds, allows to underline the different nature of the interaction between the two organic moieties considered here and the inorganic surface. Propanol binds covalently to the interlayer surface and no free molecules are present in the interlayer space. This is confirmed by the comparison of the theoretical and experimental ^{13}C-NMR chemical shifts that are in good agreement. In contrast, imidazole has a weak interaction with the surface. Nevertheless, it appears that free imidazole is not a good candidate as a proton carrier group inside such a scaffold. In fact, due to the high affinity of imidazole molecules with the acidic protons present in the interlayer space, the proton hopping between azoles is hindered by the protonation of all the nitrogen atoms by HLN protons. Adding a linker between the surface and the imidazole group could thus be an effective way to increase their distance, then favoring an efficient chain of imidazole/imidazole proton transfer.

Acknowledgments

We acknowledge funding from MIUR project FIRB2012 "INCYPIT - INnovative Ceramic and hYbrid materials for Proton conducting fuel cells at Intermediate Temperature: design, characterization and device assembly" (RBFR12CQP5), and support from CINECA through the ISCRA initiative under grant "ProTIC - Proton Transfer in hybrid Inorganic-organic Conductors" (HP10BSM76E). We thank F. Giordano (ISMN-CNR, Palermo) for the XRD measurements.

References

1 K.-D. Kreuer, S.J. Paddison, E. Spohr, M. Schuster, *Chem. Rev.*, 2004, **104**, 4637-4678.

2 P.L. Antonucci, A.S. Aricò, P. Creti, E. Ramunni, V. Antonucci, *Solid State Ionics*, 1999, **125**, 431-437.

3 K.T. Adjemian, S.J. Lee, S. Srinivasan, J. Benziger, A.B. Bocarsly, *J. Electrochem. Soc.*, 2002, **149**, A256-A261.

4 D.H. Jung, S.Y. Cho, D.H. Peck, D.R. Shin, J.S. Kim, *J. Power Sources*, 2003, **118**, 205–211.

5 H. Munakata, H. Chiba, K. Kanamura, *Solid State Ionics*, 2005, **176**, 2445–2450.

6 J.J. Smith, I. Zharov, *Chem. Mater.*, 2009, **21**, 2013–2019.

7 K. Yasumoto, T. Norisuye, Y. Teranishi, Q. Tran-Cong-Miyata, S. Nomura, *J. Polym. Sci. Part A: Polym. Chem.*, 2012, **50**, 3295–3302.

8 B. Wu, J. Pan, L. Ge, L. Wu, H. Wang, T. Xu, *Scientific Reports*, 2014, **4**, 4334.

9 C. Liang, J. Li, H. Tang, H. Zhang, H. Zhang, P. Mu, *J. Mater. Chem. A*, 2014, **2**, 753-760.

10 B. Saparov, D. B. Mitzi, *Chem. Rev.*, 2016, **116**, 4558-4596.

11 R. E. Schaak, T. E. Mallouk, *Chem. Mat.*, 2002, **14**, 1455-1471.

12 M. Dion, M. Ganne, M. Tournoux, *Mat. Res. Bull.*, 1981, **16**, 1429-1435.

13 S. Takahashi, T. Nakato, S. Hayashi, Y. Sugahara, K. Kuroda, *Inorg. Chem.*, 1995, **34**, 5065-5069.

14 H. Suzuki, K. Notsu, Y. Takeda, W. Sugimoto, Y. Sugahara, *Chem. Mater.*, 2003, **15**, 636-641.

15 A. Shimada, Y. Yoneyama, S. Tahara, P. H. Mutin, Y. Sugahara., *Chem. Mater.*, 2009, **21**, 4155-4162.

16 Y. Takeda, H. Suzuki, K. Notsu, W. Sugimoto, and Y. Sugahara, *Mat. Res. Bull.*, 2006, **41**, 834-841.

17 C. Wang, K. Tang, D. Wang, Z. Liu, L. Wang, Y. Zhu, Y. Qian, *J. Mater. Chem.*, 2012, **22**, 11086-11092.

18 J. Gopalakrishnan, V. Bhat, B. Raveau, *Mater. Res. Bull.*, 1987, **22**, 413-417.

19 T. Matsuda, M. Udagawa, I. Kunou, *J. Catal.*, 1997, **168**, 26-34.

20 F. Giannici, A. Mossuto Marculescu, A.S. Cattaneo, C. Tealdi, P. Mustarelli, A. Longo, A. Martorana, *Inorg. Chem*. 2017, **56**, 645-653.

21 R. Marschall, M. Sharifi, M. Wark, *Micropor. Mesopor. Mat.*, 2009, **123**, 21-29.

22 Z. Zhou, S. Li, Y. Zhang, M. Liu, W. Li, *J. Am. Chem. Soc.*, 2005, **127**, 10824-10825.

23 S. Bureekaew, S. Horike, M. Higuchi, M. Mizuno, T. Kawamura, D. Tanaka, N. Yanai, S. Kitagawa, S., *Nat. Mater.*, 2009, **8**, 831-836.

24 R. Dovesi, V. R. Saunders, C. Roetti, R. Orlando, C. M. Zicovich-Wilson, F. Pascale, K. Doll, N. M. Harrison, B. Civalleri, I. J. Bush, Ph. D'Arco, M. Llunell, CRYSTAL09, University of Torino, Torino, 2009.

25 R. Orlando, I. J. Bush, M. Delle Piane, P. Ugliengo, M. Ferrabone, R. Dovesi, *J. Comput. Chem.*, 2012, **33**, 2276-2284.

26 S. Di Tommaso, F. Giannici, A. Mossuto Marculescu, A. Martorana, C. Adamo, F. Labat, *J. Chem. Phys.*, 2014, **141**, 024704.

27 J. P. Perdew, K. Burke, M. Ernzerhof, *Phys. Rev. Lett.*, 1996, **77**, 3865-3868.

28 Y. Zhao, D. G. Truhlar, *J. Chem. Phys.*, 2008, **128**, 184109.

29 A. D. Becke, *J. Chem. Phys.*, 1993, **98**, 1372-1377.

30 C. Lee, W. Yang, R. G. Parr, *Phys. Rev. B*, 1988, **37**, 785-789.

31 C. Adamo, V. Barone, *J. Chem. Phys.*, 1999, **110**, 6158-6170.

32 M. Ernzerhof, G. E. Scuseria, *J. Chem. Phys.*, 1999, **110**, 5029-5036.

33 S. Grimme, *J. Comput. Chem.*, 2006, **27**, 1787-1799.

34 Basis sets have been taken from the CRYSTAL09 web site (http://www.crystal.unito.it/Basis_Sets/Ptable.html)

35 P. Durand, J. C. Barthelat, *Theor. Chim. Acta*, 1975, **38**, 283-302.

36 M. F. Peintinger, D. Vilela Oliveira, T. Bredow, *J. Comput. Chem.*, 2013, **34**, 451-459.

37 R. Dovesi, M. Causà, R.Orlando, C.Roetti, V. R. Saunders, *J. Chem. Phys.*, 1990, **92**, 7402.

38 Gaussian 09, Revision A.02, M. J. Frisch, G. W. Trucks, H. B. Schlegel, G. E. Scuseria, M. A. Robb, J. R. Cheeseman, G. Scalmani, V. Barone, B. Mennucci, G. A. Petersson, H. Nakatsuji, M. Caricato, X. Li, H. P. Hratchian, A. F. Izmaylov, J. Bloino, G. Zheng, J. L. Sonnenberg, M. Hada, M. Ehara, K. Toyota, R. Fukuda, J. Hasegawa, M. Ishida, T. Nakajima, Y. Honda, O. Kitao, H. Nakai, T. Vreven, J. A. Montgomery Jr., J. E. Peralta, F. Ogliaro, M. Bearpark, J. J. Heyd, E. Brothers, K. N. Kudin, V. N. Staroverov, R. Kobayashi, J. Normand, K. Raghavachari, A. Rendell, J. C. Burant, S. S. Iyengar, J. Tomasi, M. Cossi, N. Rega, J. M. Millam, M. Klene, J. E. Knox, J. B. Cross, V. Bakken, C. Adamo, J. Jaramillo, R. Gomperts, R. E. Stratmann, O. Yazyev, A. J. Austin, R. Cammi, C. Pomelli, J. W. Ochterski, R. L. Martin, K. Morokuma, V. G. Zakrzewski, G. A. Voth, P. Salvador, J. J. Dannenberg, S. Dapprich, A. D. Daniels, Ö. Farkas, J. B. Foresman, J. V. Ortiz, J. Cioslowski and D. J. Fox, Gaussian, Inc.,Wallingford CT, 2009.

39 K. Wolinski, J. F. Hilton, P. Pulay, *J. Am. Chem. Soc.*, 1990, **112**, 8251-8260.

40 W. Kutzelnigg, U. Fleischer, M. Schindler, *NMR Basic Principles and Progress*, Springer Verlag, Berlin/Heidelberg, 1991, **213**, 165-262.

41 P. J. Hay and W. R. Wadt, *J. Chem. Phys.*, 1985, **82**, 270-283.

42 B. Henry, P. Tekely, J.-J. Delpuech, *J. Am. Chem. Soc.*, 2002, **124**, 2025-2034.

43 Y. Kobayashi, M. Tian, M. Eguchi, T. E. Mallouk, *J. Am. Chem. Soc.*, 2009, **131**, 9849-9855.

44 C. Ricca, A. Ringuedé, M. Cassir, C. Adamo, F. Labat, *J. Comp. Chem.*, 2015, **36**, 9-21.

45 A. Szemjonov, T. Pauporté, I. Ciofini, F. Labat, *Phys. Chem. Chem. Phys.*, 2014, **16**, 23251-23259.

46 C. Adamo, V. Barone, *Chem. Phys. Lett.*, 1998, **298**, 113-119.

47 Z. Zhou, R. Liu, J. Wang, S. Li, M. Liu, J. L. Brédas, *J. Phys. Chem. A*, 2006, **110**, 2322-2324.

48 G. F. Mangiatordi, V. Butera, N. Russo, D. Laage, C. Adamo, *Phys. Chem. Chem. Phys.*, 2012, **14**, 10910-10918.

49 G. F. Mangiatordi, D. Laage, C. Adamo, *J. Mat. Chem. A*, 2013, **1**, 7751-7759.

50 D. Basak, C. Versek, J. A. Harvey, S. Christensen, J. Hillen, S. M. Auerbach, M. T. Tuominen, D. Venkataraman, *J. Mater. Chem.*, 2012, **22**, 20410-20417.

Table 1. Optimized (B3LYP) lattice parameters (*a*, *b*, *c* in Å and *α*, *β*, *γ* in degrees) of propanol and imidazole substituted HLN in the bulk models mono-substituted (**Pro-HLN*b***) and **Imi-HLN*b***) and di-substituted (2**Pro-HLN*b*** and 2**Imi-HLN*b***) for different coverage values (θ).

	HLN[a]	**Pro-HLN*b*** θ = 0.25	**2Pro-HLN*b*** θ = 0.34	**2Pro-HLN*b*** θ = 0.50	**Imi-HLN*b*** θ = 0.25	**2Imi-HLN*b*** θ = 0.34
a	3.957	7.924	11.880	7.878	7.926	11.878
b	3.957	7.860	7.881	7.925	7.863	7.872
c	10.421	13.509	14.379	14.126	13.982	13.537
α	90.0	95.76	94.85	99.12	103.57	89.75
β	90.0	91.88	94.48	72.82	86.00	85.94
γ	90.0	89.98	90.01	89.96	90.01	89.94

a) from reference 26

Table 2. Computed Nb-O bonds (in Å). Niobium atoms in green, oxygen atoms in red

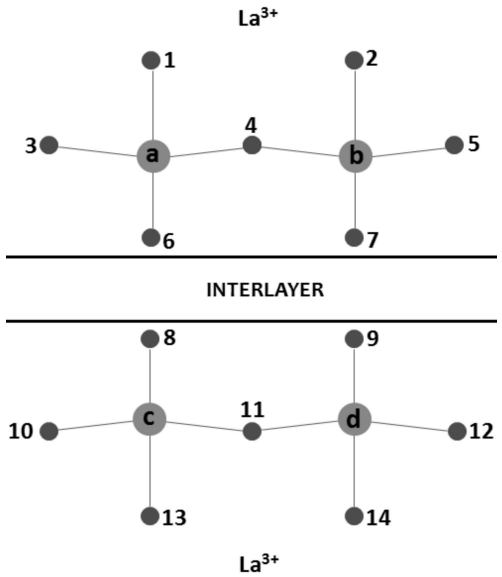

Species	bond	equatorial		axial-long		axial-short	
H	average	2.005		2.212		1.795	
	min	**a-3, a-4**	1.999	**a-1**	2.162	**a-6**	1.813
	max	**c-10, c-11**	2.011	**c-13**	2.261	**c-8**	1.776
Pro-HLN$_b$[a]	average	2.039		2.289		1.819	
	min	**b-4**	2.026	**b-2**	2.096	**d-9**	1.764
	max	**a-3, a-4**	2.046	**d-14**	2.487	**b-7**	1.887
2Pro-HLN$_b$[b] (θ=0.50)	average	2.037		2.276		1.816	
	min	**b-4**	2.025	**b-2, c-13**	2.125	**a-6**	1.770
	max	**d-12**	2.045	**a-1**	2.430	**c-8**	1.865
Imi-HLN$_b$	average	2.029		2.269		1.835	
	min	**d-11**	1.935	**d-14**	2.088	**b-7**	1.775
	max	**d-12**	2.130	**c-13**	2.456	**d-9**	1.895
2Imi-HLN$_b$	average	2.040		2.286		1.812	
	min	**d-11**	2.010	**d-14**	2.093	**a-6**	1.764
	man	**a-4**	2.058	**b-2**	2.421	**d-9**	1.907

a) The propyl group is bound to oxygen 8; b) The two propyl groups are bound to oxygen 8 and 7.

Table 3. Experimental and computed (B3LYP/IGLO-III) ^{13}C chemical shifts (*ppm*) of **Pro-HLN** and **Imi-HLN** with respect to tetramethylsilane (TMS) absorption, computed for different clusters. See Figure 2 for carbon labeling.

	CLUSTER 1	**CLUSTER 2**	**CLUSTER 3**	**EXP**
Pro-HLN				
C1	89.7	83.2	83.2	81.0
C2	34.4	32.5	29.3	26.0
C3	16.8	13.0	13.3	12.5
Imi-HLN				
C2	138.42	165.74	148.42	130 - 137
C4	128.80	132.11	134.11	116 - 124
C5	130.34	116.77	106.69	116 - 124

Table 4. Selected angles (in degrees) of the optimized (B3LYP) structures of **Imi-HLN*b*** and **2Imi-HLN*b***.

	Imi-HLN*s*	**Imi-HLN*b***	**2Imi-HLN*b***	
			first imidazole	second imidazole
Nb-O-H-N1	14.66	90.75	26.90	8.03
Nb-O-N1-C3	33.45	84.08	102.22	110.45
Nb-O-N1	147.20	150.00	147.20	137.50
O-N1-N2	117.52	156.56	156.48	161.91

Figure caption

Figure1. XRD patterns of HLN, **Pro-HLN** and **Imi-HLN**.

Figure 2. ^{13}C-NMR of a) **Pro-HLN** and b) **Imi-HLN**.

Figure 3. Sketch of the structural models, *surface* and *bulk*, considered in this work for the characterization of functionalized HLN.

Figure 4. Optimized structures (B3LYP) of **Pro-HLN** and **Imi-HLN** in their *surface* and *bulk* models (mono and di-substituted).

Figure 5. Total and partial density of states computed for **Pro-HLN$_b$** and **Imi-HLN$_b$** at the B3LYP level. The Fermi level (E_F) is set at 0 eV.

Figure 6. Structure of the clusters 1, 2 and 3 (B3LYP) used to compute the 13C-NMR shielding for **Pro-HLN** and **Imi-HLN**.

Figure 1

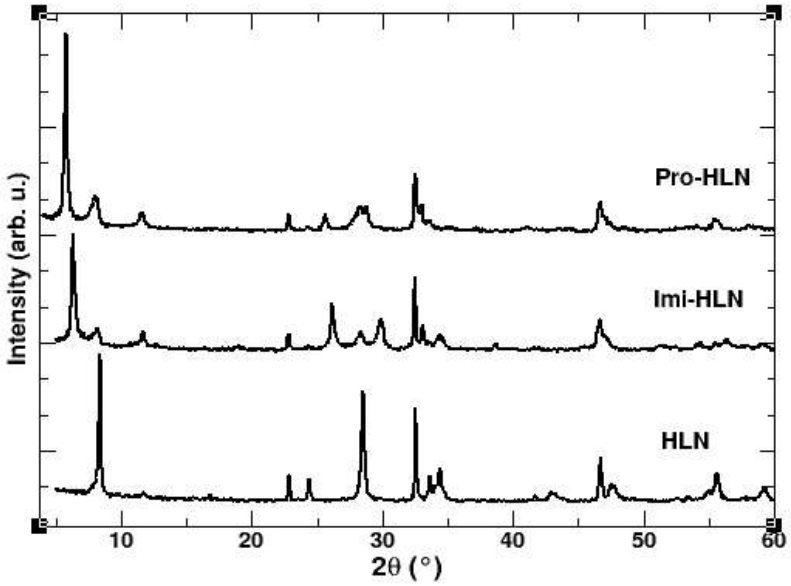

Figure 2

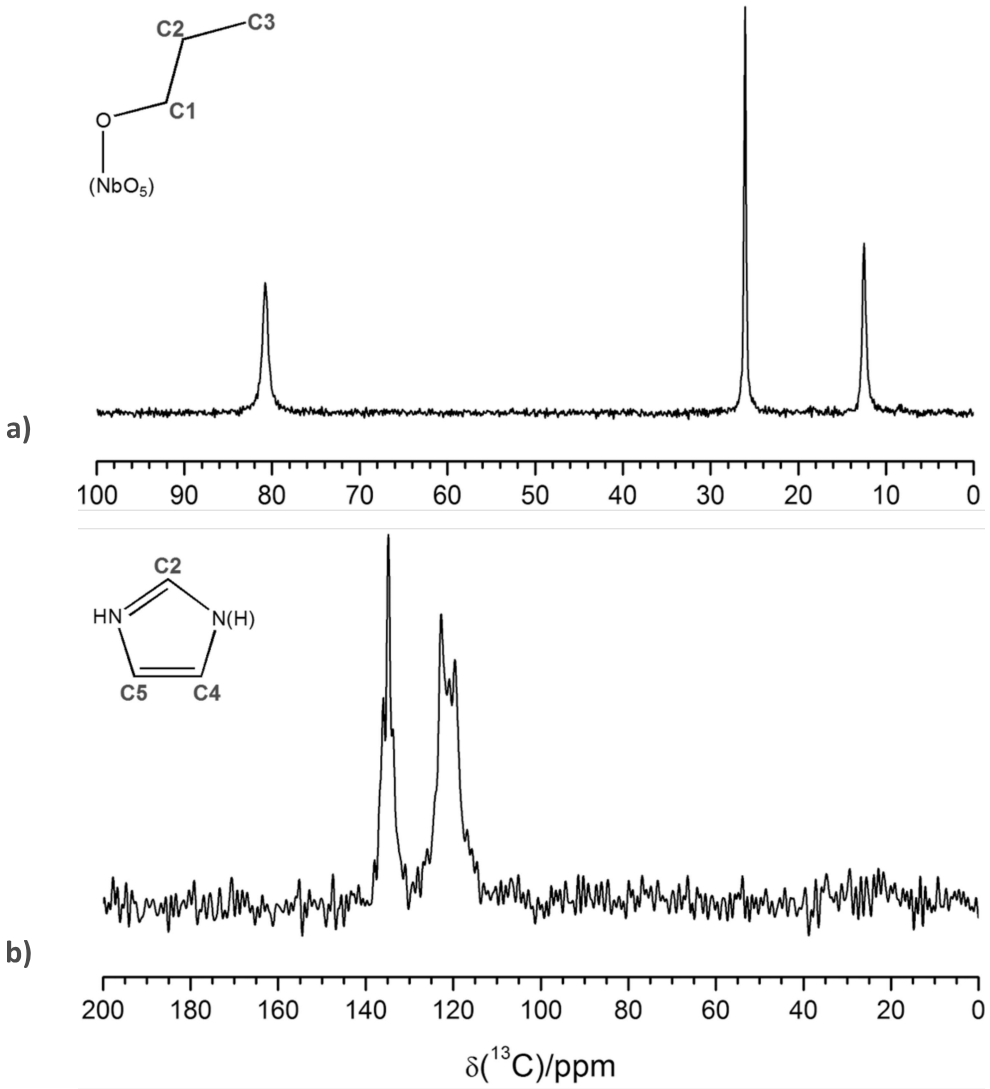
C2
C3
C1
O
(NbO5)
a)
100
90
80
70
60
50
40
30
20
10
0
C2
HN
N(H)
C5
C4
b)
200
180
160
140
120
100
80
60
40
20
0
δ(13C)/ppm

Figure 3

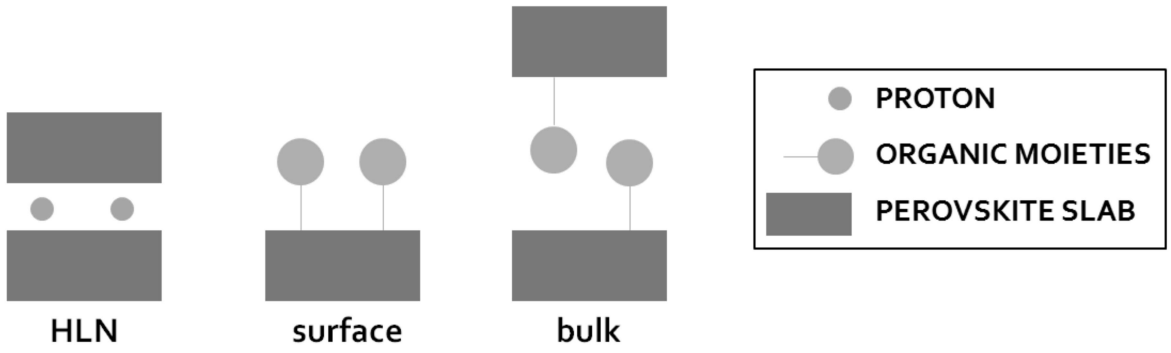

Figure 4.

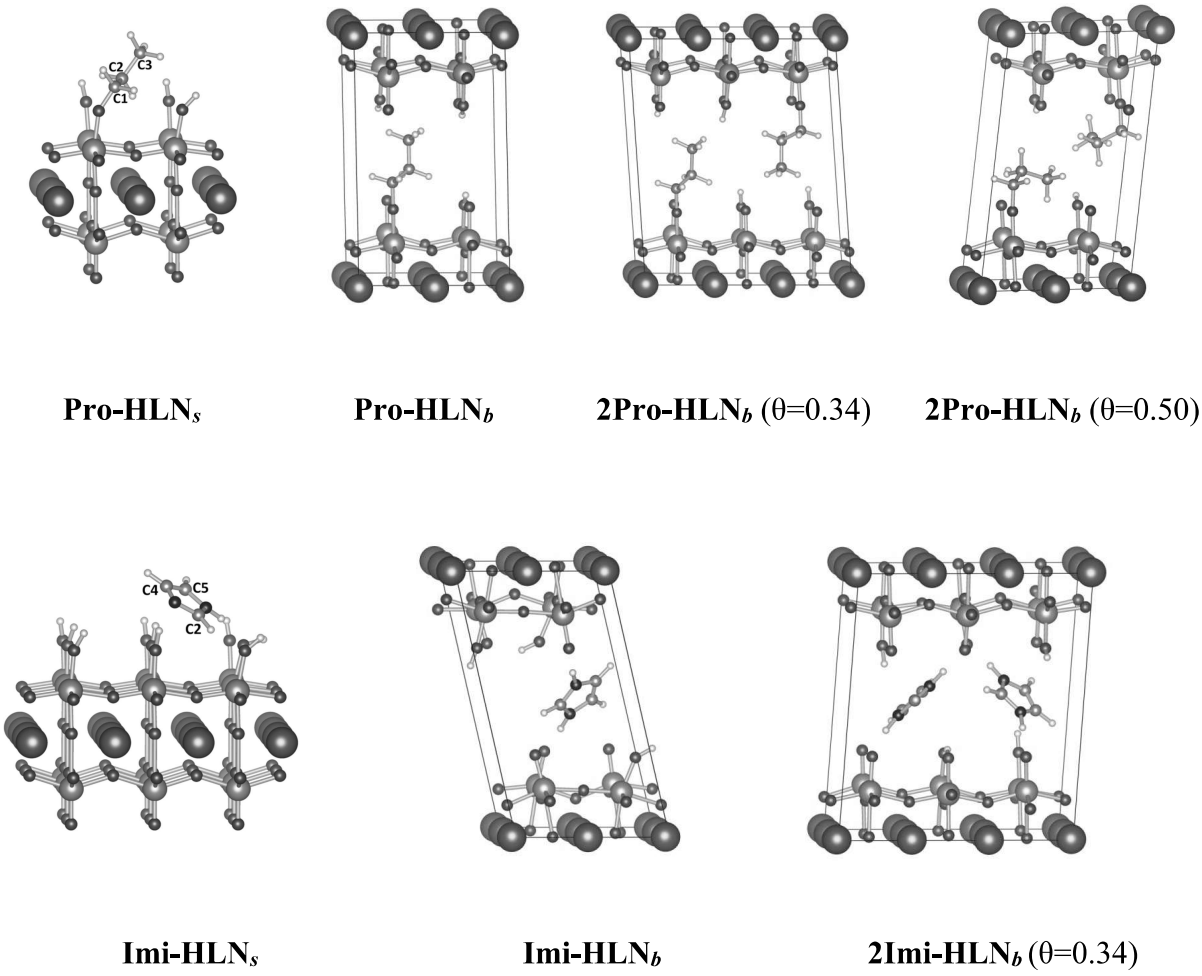

Pro-HLN$_s$ **Pro-HLN**$_b$ **2Pro-HLN**$_b$ (θ=0.34) **2Pro-HLN**$_b$ (θ=0.50)

Imi-HLN$_s$ **Imi-HLN**$_b$ **2Imi-HLN**$_b$ (θ=0.34)

Figure 5

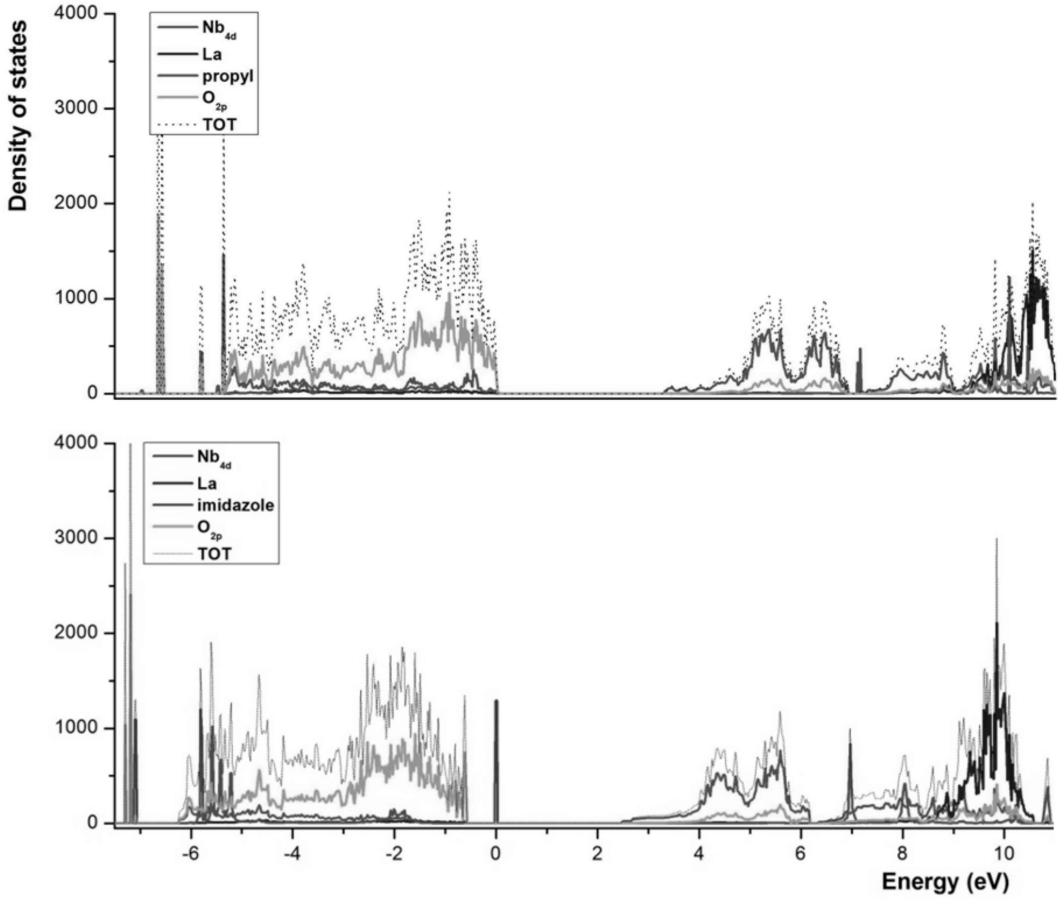
Density of states
4000
3000
2000
1000
0
Nb4d
La
propyl
O2p
TOT
imidazole
-6
-4
-2
0
2
4
6
8
10
Energy (eV)

Figure 6